

A FEATURE MATCHING-BASED APPROACH TO DEFORMATION FIELDS MEASUREMENT FROM MR IMAGES OF NON-RIGID OBJECT

PENGLIN ZHANG^{1,2}

¹Department of Robotics
Ritsumeikan University

Noji-higashi 1-1-1, Kusatsu, Shiga 525-8577, Japan
zpl@se.ritsumei.ac.jp

²School of remote sensing and information engineering
Wuhan University, Wuhan, China
zplcy@263.net

SHINICHI HIRAI¹ AND KAZUMI ENDO¹

¹Department of Robotics
Ritsumeikan University

Noji-higashi 1-1-1, Kusatsu, Shiga 525-8577, Japan
hirai@se.ritsumei.ac.jp; rr001026@se.ritsumei.ac.jp

ABSTRACT. *Though a variety of different algorithms have been implemented for estimation of the deformation fields of biological tissue from magnetic resonance (MR) images, few attempts in feature tracking areas have been reported. In this study, we propose a method to measure deformation fields of biological tissues based on local feature tracking. First, we use correlation score (cs) based method to obtain a candidate matches set. Next, relaxation technique is used to disambiguate matches. Third, the dense deformation fields is calculated using linear interpolation approach within Delaunay triangles net. To test the validity of our approach, we applied the proposed approach to MR images of a volunteer's calf. Moreover, the reverse movement of selected check points was used to evaluate the reliability and accuracy of the result. Preliminary experiment results of this paper reveal that the proposed approach is feasible.*

Keywords: Feature tracking, MR image, Deformation fields

1. Introduction. Since its initial use for human imaging over 20 years ago, magnetic resonance imaging (MRI) has become a widely used clinical imaging modality [1]. MRI has increasingly employed in biomedical applications. As one of research branches in MR image processing, interior deformation fields measurement is very important for physical parameters estimation. The purpose of this paper is to develop a valid approach for measurement the dense deformation fields of non-rigid and non-uniform object. The input data of this procedure is MR images before and after deformation.

Though there has been significant growth on deformation fields measurement from medical MR images, most works have been done are mainly focus on non-rigid registration approaches. Especially, many proposed approaches are based on elastic deformable model[2-10]. Generally, the deformable models can be classified in two basic categories: parametric and geometric deformable models [5]. Parametric deformable models, also

called snakes, was first proposed by Kass, Witkin and Terzopoulos in 1987 [11]. Parametric deformable models represent curves and surfaces explicitly in their parametric forms during deformation. Usually, it must formulate an energy function for a deformable contour in order to find a parameterized curve that minimizes the weighted sum of internal energy and potential energy. Different from parametric deformable models, geometric deformable models are based on curve evolution theory and the level set method, representing curves and surfaces implicitly as a level set of a higher-dimensional scalar function. Their parameterizations are computed only after complete deformation, this allowing topological adaptivity to be easily accommodated [12]. In deformable models, the motion fields of deformable contour or surface can be regarded as the deformation fields.

Though the deformable models undergo a significant development, and are widely used in image segmentation, non-rigid registration and deformation fields measurement, they still have some limitations. Typically, for parametric approach, the difference between the initial model and the desired object boundary will directly affect the final result. Moreover, it has difficulty dealing with topological adaptation such as splitting or merging model parts, a useful property for recovering either multiple objects or an object with unknown topology. Although geometric approach can address the topological adaptation using curve evolution theory, it may generate shapes that have inconsistent topology with respect to the actual object, when applied to noisy images with significant boundary gaps [12]. Furthermore, the most important issue of deformable models in deformation fields measurement is that they cannot deal with the interior deformation fields measurement.

In this paper, we propose a feature matching-based approach to measure sparse local deformation fields from MR images of non-rigid non-uniform biological tissues. By means of linear interpolation, the interior dense deformation fields at different regions of an object are interpolated using local deformation fields on the nodes of an irregular Delaunay triangle net. In this case, certain numbers of high curvature feature points (also called points of interest) in the initial and deformed MR volumetric images are first pre-extracted to form two feature points sets. Then, we apply the proposed feature matching method into the two feature points sets in order to find feature pairs homologous each other. The local deformation fields are computed from the obtained homologous feature point pairs.

This paper is organised as follows. Section 2 gives overview of the proposed approach. Section 3 describes interior deformation fields measurement from MR images. Section 4 presents examples and the results of preliminary experiments. The final section presents our discussion and conclusions.

2. Overview of the Proposed Approach. The pipeline of our approach is shown in Figure 1. At the initial phase, Harris operator [13] is used to automatically extract high curvature points of interest from the initial and deformed MR images as reference features. The purpose of *absolute orientation* is to find the geometric relationship between deformed MR image and the initial one. Many approaches have been reported to address this problem. For example, a mutual information based non-rigid registration approach [19] was proposed to find geometric transformation parameters in order to align two medical images. In this paper, we use an unit quaternion method [14][15] to find the

solution of the transformation parameters of two systems: rotation matrix \mathcal{R} and translation vector $\boldsymbol{\tau}$. This mainly comes from: 1) there is a rigid region (bone) in experiment data; 2) we have already extracted rigid feature points around bone, which are useful for finding geometric transform parameters by means of unit quaternion approach.

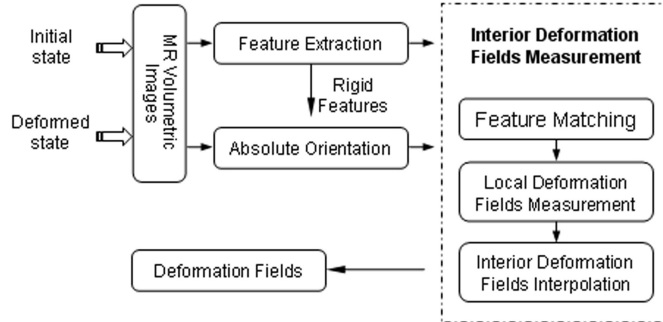


FIGURE 1. Pipeline of the proposed approach

Before obtaining the dense deformation fields, we must track the precise corresponding position in the deformed MR image for a given feature point of interest in the initial MR image. In this paper, we propose a *correlation score* based robust algorithm to obtain homologous point pairs.

The obtained point matches are used to measure the local deformation fields at the corresponding location under a global coordinate system. Subsequently, in order to calculate the dense deformation fields, we propose to infer the interior dense deformation fields using sparse local deformation fields at the nodes of Delaunay triangles.

Finally, the reverse movement of selected check points is used to evaluate the reliability of obtained dense deformation fields. When the check points in the deformed image can move back to their original position in the initial image, it implies that the obtained deformation fields is reliable and accurate.

3. Interior Deformation Measurement from MR Images. This section presents how to measure interior deformation of non-rigid non-uniform object by means of the proposed approach. Concisely, we first try to obtain a potential matches set (PMS) through a robust feature matching algorithm (two steps feature matching algorithm). Whereafter, interior deformation is calculated using interpolation algorithm in Delaunay triangles.

3.1. Feature matching. A) *First matching.* Let $\mathbf{x} = [x \ y]^T$ be the coordinates of an MR image, \mathbf{p}_1 be feature point in the initial MR image, and \mathbf{p}_2 be the projection of \mathbf{p}_1 in the deformed MR image. Then, the position of \mathbf{p}_2 can be calculated using affine transformation with rotation matrix \mathcal{R} and translation vector $\boldsymbol{\tau}$ as follows:

$$\mathbf{x}_{\mathbf{p}_2} = \mathcal{R}\mathbf{x}_{\mathbf{p}_1} + \boldsymbol{\tau}, \quad (1)$$

where $\mathbf{x}_{\mathbf{p}_1} = [x_1, y_1]^T$ and $\mathbf{x}_{\mathbf{p}_2} = [x_2, y_2]^T$ are coordinates of point \mathbf{p}_1 and \mathbf{p}_2 , respectively.

Let us introduce the following rectangular region for matching:

$$\mathcal{C}_m = \{\mathbf{x} = [x \ y]^T | x \in [-m, m], y \in [-n, n]\}. \quad (2)$$

The size of this region is given by $|\mathbf{C}_m| = (2m + 1)(2n + 1)$. Let $g(\mathbf{x})$ and $g'(\mathbf{x})$ be the intensity of the initial and deformed MR images at position \mathbf{x} . Let $\bar{g}_{\mathbf{p}_1}$ and $\bar{g}'_{\mathbf{p}_2}$ be the means of intensity in the rectangular region \mathbf{C}_m around \mathbf{p}_1 in the initial image and \mathbf{p}_2 in the deformed image:

$$\bar{g}_{\mathbf{p}_1} = \frac{1}{|\mathbf{C}_m|} \sum_{\mathbf{x} \in \mathbf{C}_m} g(\mathbf{p}_1 + \mathbf{x}), \quad \bar{g}'_{\mathbf{p}_2} = \frac{1}{|\mathbf{C}_m|} \sum_{\mathbf{x} \in \mathbf{C}_m} g'(\mathbf{p}_2 + \mathbf{x}), \quad (3)$$

Let $\sigma(g_{\mathbf{p}_1})$ and $\sigma(g_{\mathbf{p}_2})$ be the standard derivation of the rectangular region \mathbf{C}_m around \mathbf{p}_1 in the initial image and \mathbf{p}_2 in the deformed image, respectively. The correlation score between feature points \mathbf{p}_1 and \mathbf{p}_2 can be calculated using match regions around them, which is given by

$$cs(\mathbf{p}_1, \mathbf{p}_2) = \frac{\sum_{\mathbf{x} \in \mathbf{C}_m} (g(\mathbf{p}_1 + \mathbf{x}) - \bar{g}_{\mathbf{p}_1})(g'(\mathbf{p}_2 + \mathbf{x}) - \bar{g}'_{\mathbf{p}_2})}{|\mathbf{C}_m| \sigma(g_{\mathbf{p}_1}) \times \sigma(g_{\mathbf{p}_2})} \quad (4)$$

Through first matching stage, a point matches set with many-to-many relationships is obtained. Namely, a point in the initial MR image may be paired not less than one points (we called candidate matches) in the deformed MR image, and vice versa. Therefore, the first matching based on correlation score only is rough and insufficient. To disambiguate the matches and obtain potential matches set (PMS), relaxation technique is introduced in the following section. Here, pair $(\mathbf{p}_1, \mathbf{p}_2)$ be regarded as a potential match if and only if \mathbf{p}_2 is the best candidate match of \mathbf{p}_1 , and \mathbf{p}_1 also is the best candidate match of \mathbf{p}_2 .

B) Relaxation labeling. The idea of relaxation technique is to use iterated local context updates to achieve a globally consistent result [16]. One of the key issues of relaxation algorithm is to design a valid cost function in order to control the convergence rate. Let $SM(\mathbf{p}_{1_i}, \mathbf{p}_{2_j})$ be the strength of match $(\mathbf{p}_{1_i}, \mathbf{p}_{2_j})$. Cost function ε is given by the average of strength of match (SM) as follows:

$$\varepsilon = \frac{1}{N_t} \sum_{i,j=1}^{N_t} SM(\mathbf{p}_{1_i}, \mathbf{p}_{2_j}) \quad (5)$$

where N_t is the total number of matches in PMS, \mathbf{p}_{1_i} represents the i -th point in the initial image, and \mathbf{p}_{2_j} represents the j -th candidate match of \mathbf{p}_{1_i} .

Let $\mathcal{N}(\mathbf{p}_{1_i})$ and $\mathcal{N}(\mathbf{p}_{2_j})$ be the neighbors of point \mathbf{p}_{1_i} and \mathbf{p}_{2_j} within a circle, respectively. We expect many potential matches $(\mathbf{n}_{1_k}, \mathbf{n}_{2_l})$ if and only if $(\mathbf{p}_{1_i}, \mathbf{p}_{2_j})$ is a potential match, where $\mathbf{n}_{1_k} \in \mathcal{N}(\mathbf{p}_{1_i})$ and $\mathbf{n}_{2_l} \in \mathcal{N}(\mathbf{p}_{2_j})$. Otherwise, we expect only a few, or even none at all. Then, referring to the strength of match function proposed in [17], we define the SM function between \mathbf{p}_{1_i} and \mathbf{p}_{2_j} as:

$$SM(\mathbf{p}_{1_i}, \mathbf{p}_{2_j}) = cs(\mathbf{p}_{1_i}, \mathbf{p}_{2_j}) + \sum_{\substack{\mathbf{n}_{1_k} \in \mathcal{N}(\mathbf{p}_{1_i}) \\ \mathbf{n}_{2_l} \in \mathcal{N}(\mathbf{p}_{2_j})}} cs(\mathbf{n}_{1_k}, \mathbf{n}_{2_l}) \cdot e^{-\mathcal{J}(\mathbf{p}_{1_i}, \mathbf{p}_{2_j}; \mathbf{n}_{1_k}, \mathbf{n}_{2_l})}, \quad (6)$$

Theoretically, if $(\mathbf{p}_{1_i}, \mathbf{p}_{2_j})$ is a potential match, and that $(\mathbf{n}_{1_k}, \mathbf{n}_{2_l})$ with $\mathbf{n}_{1_k} \in \mathcal{N}(\mathbf{p}_{1_i})$ and $\mathbf{n}_{2_l} \in \mathcal{N}(\mathbf{p}_{2_j})$ also is a potential match, then the following two are satisfied: 1) the distance between \mathbf{n}_{1_k} and \mathbf{p}_{1_i} in the initial image should close or even equal to the distance between \mathbf{n}_{2_l} and \mathbf{p}_{2_j} in the deformed image, and 2) the deformation direction of \mathbf{p}_{1_i} should close or even identical to the deformation direction of \mathbf{n}_{1_k} , due to they are

in a local region. Taking account of the above two in SM function, let us introduce the relative distance difference and direction constraint.

Let $d(\mathbf{p}_{1_i}, \mathbf{n}_{1_k})$ be Euclidean distance between \mathbf{p}_{1_i} and \mathbf{n}_{1_k} in the initial image, $d(\mathbf{p}_{2_j}, \mathbf{n}_{2_l})$ be Euclidean distance between \mathbf{p}_{2_j} and \mathbf{n}_{2_l} in the deformed image. According to [18], the relative distance difference $dist(\mathbf{p}_{1_i}, \mathbf{p}_{2_j}; \mathbf{n}_{1_k}, \mathbf{n}_{2_l})$ between $d(\mathbf{p}_{1_i}, \mathbf{n}_{1_k})$ and $d(\mathbf{p}_{2_j}, \mathbf{n}_{2_l})$ is given by

$$dist(\mathbf{p}_{1_i}, \mathbf{p}_{2_j}; \mathbf{n}_{1_k}, \mathbf{n}_{2_l}) = 1 + \frac{2|d(\mathbf{p}_{1_i}, \mathbf{n}_{1_k}) - d(\mathbf{p}_{2_j}, \mathbf{n}_{2_l})|}{d(\mathbf{p}_{1_i}, \mathbf{n}_{1_k}) + d(\mathbf{p}_{2_j}, \mathbf{n}_{2_l})}. \quad (7)$$

Moreover, let notation $\overrightarrow{\mathbf{p}_{1_i}\mathbf{p}_{2_j}}$ be the vector from \mathbf{p}_{1_i} to its corresponding position \mathbf{p}_{2_j} , $\overrightarrow{\mathbf{n}_{1_k}\mathbf{n}_{2_l}}$ be the vector from \mathbf{n}_{1_k} to its corresponding position \mathbf{n}_{2_l} , and $\mathcal{O}(\overrightarrow{\mathbf{p}_{1_i}\mathbf{p}_{2_j}}, \overrightarrow{\mathbf{n}_{1_k}\mathbf{n}_{2_l}})$ be the angle between vector $\overrightarrow{\mathbf{p}_{1_i}\mathbf{p}_{2_j}}$ and $\overrightarrow{\mathbf{n}_{1_k}\mathbf{n}_{2_l}}$. Then, the $\mathcal{O}(\overrightarrow{\mathbf{p}_{1_i}\mathbf{p}_{2_j}}, \overrightarrow{\mathbf{n}_{1_k}\mathbf{n}_{2_l}})$ is given by

$$\mathcal{O}(\overrightarrow{\mathbf{p}_{1_i}\mathbf{p}_{2_j}}, \overrightarrow{\mathbf{n}_{1_k}\mathbf{n}_{2_l}}) = 1 + \frac{1}{1 + \cos \theta} \quad (8)$$

where θ represents the angle between vector $\overrightarrow{\mathbf{p}_{1_i}\mathbf{p}_{2_j}}$ and $\overrightarrow{\mathbf{n}_{1_k}\mathbf{n}_{2_l}}$.

So far, we have already obtained the relative distance difference factor $dist(\cdot)$ and deformation direction factor $\mathcal{O}(\cdot)$, the term $\mathcal{J}(\mathbf{n}_{1_k}, \mathbf{n}_{2_l})$ in SM function (6) is then defined as

$$\mathcal{J}(\mathbf{p}_{1_i}, \mathbf{p}_{2_j}; \mathbf{n}_{1_k}, \mathbf{n}_{2_l}) = \mathcal{O}(\overrightarrow{\mathbf{p}_{1_i}\mathbf{p}_{2_j}}, \overrightarrow{\mathbf{n}_{1_k}\mathbf{n}_{2_l}}) \cdot dist(\mathbf{p}_{1_i}, \mathbf{p}_{2_j}; \mathbf{n}_{1_k}, \mathbf{n}_{2_l}). \quad (9)$$

It is noting that comparison with the similar SM function in [17]. This paper introduces the local deformation direction information to improve the robustness of SM function, especially, in the non-uniform heterogeneous object. Because the deformation direction are different in different regions, pairs' deformation direction close to the direction of candidate match must obtain larger weight for candidate match's SM computation, and vice versa. For example, in Figure 2, pairs $(\mathbf{n}_{1_2}, \mathbf{n}_{2_2})$ and $(\mathbf{n}_{1_3}, \mathbf{n}_{2_3})$ must obtain lower weight than the others in $SM(\mathbf{p}_{1_i}, \mathbf{p}_{2_j})$ computation, since the deformation direction of these two pairs is opposite to that of the candidate match $(\mathbf{p}_{1_i}, \mathbf{p}_{2_j})$.

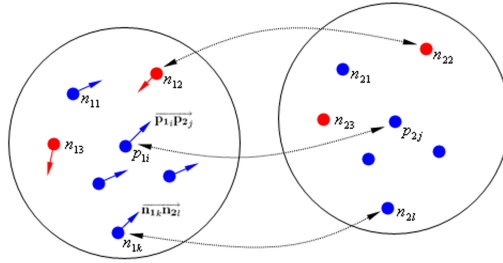


FIGURE 2. Pairs within neighbors of candidate match $(\mathbf{p}_{1_i}, \mathbf{p}_{2_j})$

In this paper, we use the same relaxation labeling implementation procedure introduced in [15]. The result of performing the above feature matching algorithm is that a PMS is obtained, which will be used to measure local sparse deformation fields and to infer the dense interior deformation fields of a non-uniform object.

3.2. Deformation Fields Measurement. We propose a Delaunay triangle based linear interpolation approach to obtain the dense deformation fields of an image. First, we use feature points in the initial (or deformed) MR image and obtain corresponding feature points in the PMS to construct Delaunay triangle net. The deformation fields of pixels inside a triangle are computed using the deformation fields of the triangle's nodes.

Let m be the number of triangles, $j = 0, 1, \dots, m-1$ be the index of triangles, $k = 1, 2, 3$ be the node number of a triangle and $\mathcal{D}_{j,k}$ be displacement vector of the k -th node of triangle j . Then, $\mathcal{D}_{j,k}$ is given by

$$\mathcal{D}_{j,k} = \mathcal{R}\mathbf{x}_{j,k} + \boldsymbol{\tau} - \mathbf{x}'_{j,k}, \quad (10)$$

where $\mathbf{x}_{j,k} = [x, y]^T$ be the position of the k -th node of triangle j in the initial image, which corresponds the position vector in the deformed MR image $\mathbf{x}'_{j,k} = [x', y']^T$. Let us define function w_k on triangle $\Delta(j)$. Assume that the area of the triangle is positive. Let \mathbf{p}_i be an arbitrary point within the triangle $\Delta(j)$. The ratio between areas of $\Delta(\mathbf{p}_i, \mathbf{p}_{\bar{k}})$ and $\Delta(j)$ determines the function:

$$w_k = \frac{\Delta(\mathbf{p}_i, \mathbf{p}_{\bar{k}})}{\Delta(j)} \quad (11)$$

where $\Delta(\mathbf{p}_i, \mathbf{p}_{\bar{k}})$ represents the triangle consists of point \mathbf{p}_i and two nodes except the k -th node of the triangle $\Delta(j)$. The displacement vector \mathcal{D}_j of the pixels within triangle $\Delta(j)$ is given by

$$\mathcal{D}_j = \sum_{k=1}^3 w_k \mathcal{D}_{j,k}. \quad (12)$$

4. Experiments and Results. Several practical examples were designed to demonstrate the capabilities of the proposed approach. First, we applied the proposed approach to the MR images sampled from a volunteer's calf using an MRI scanner at different times and different status (initial and deformed). In both cases, FOV was 20×20 cm, and the slice gap was 2 mm. In this example, we selected two slices sampled at same location before and after deformation (Figure 3) as the input data and performed the proposed feature matching approach on them. To compare with the similar feature matching algorithm, we also applied the robust feature matching (RFM) algorithm proposed by Chen [17] to the same data under same experiment conditions. Table 1 shows the numeric result of feature points matching using two approaches.

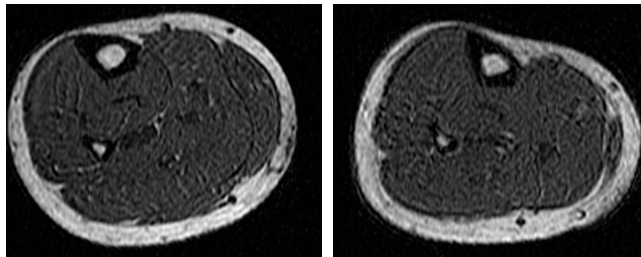


FIGURE 3. Input data of the example (Left: Initial slice. Right: Deformed slice)

TABLE 1. Error of the checking points (NOTE: TPA, the proposed approach; FPS, feature points; ITs, iteration times; T, cost time in seconds.)

Approaches	FPS in initial slice	FPS in deformed slice	α	matches in PMS	ITs	T
TPA	200	240	\	72	101	5
RFM	200	240	10	63	101	5

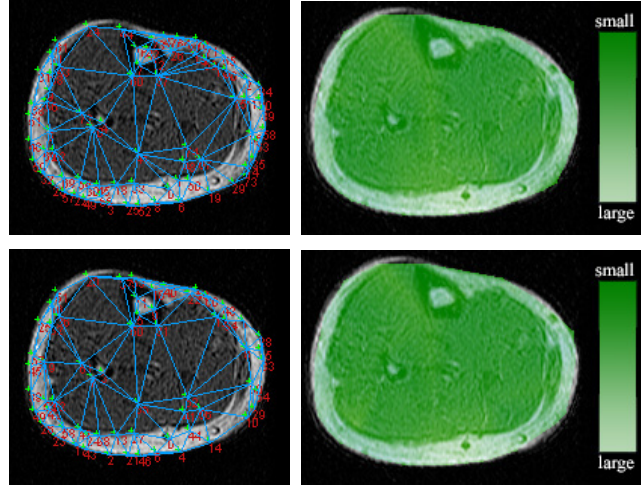


FIGURE 4. Inferred deformation fields (Left: Irregular Delaunay triangles. Right: Dense deformation fields overlaid on deformed slice. Top: result of the proposed approach. Down: result of RFM)

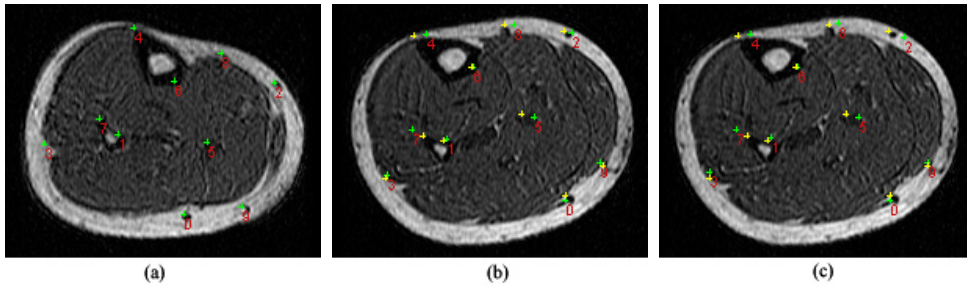


FIGURE 5. Deformation fields evaluation ((a) initial position of check points in deformed slice. (b) the reverse movement result using the deformation fields obtained by the proposed approach. (c) reverse movement result using the deformation fields obtained by RFM; Yellow cross, the original position of check points. Green cross, the reverse movement result of check points using dense deformation fields)

Table 1 indicates that the proposed approach can obtain more matches than RFM under the same conditions, in spite of it cost more time than RFM. The later results (Fig.5 and Table 2) show that the proposed approach has higher accuracy than RFM.

Secondly, to obtain the dense deformation fields, we calculated the sparse deformation fields correspond to the matches obtained previously using two approaches. Then, we constructed the irregular Delaunay triangle net, and performed the proposed linear interpolation approach to obtain the dense deformation fields. Figure 4 shows the delaunay triangle net and the dense deformation fields overlaid on the deformed slice. The delaunay triangle net was constructed using feature points obtained PMS. The deformation fields are obtained using the two set of sparse deformation fields introduced above. In Figure 4, the green color correspond to small deformation area, and yellow color correspond to the large deformation area.

Finally, to evaluate the reliability and precision of the estimated deformation field, we selected 10 obvious points (Figure 5(a)) which can be observed easily. Then, performing reverse movement using the invert deformation fields of obtained deformation fields on these check points, we observe if they can move back to the initial position in the initial slice. Figure 5(b) and (c) illustrate the movement result of 10 check points. In Figure 5(b) and (c), yellow cross illustrate the original position of check points, and green one illustrate the projections of reverse movement result of the check points in the deformed MR slice. As shown in Figure 4, most of the check points can go back to their original position in the two approaches, implying that the estimated deformation field is reliable. To evaluate the accuracy, the distance between the location of a check point after performing reverse movement and its actually original location is used to measure the error of the check point. Accordingly, the root mean square error (RMSE) of these check points also are computed to evaluate the accuracy of obtained deformation. Table 2 gives the error of selected 10 check points and RMSE, respectively. In Table 2, there are only two check points (4, 5 and 7) whose error over 0.2 in the proposed approach, but, there are four check points (2, 4, 5 and 7) whose error over 0.2 in RFM approach, this illustrate the deformation fields obtained using the proposed approach more reliable than that obtained using RFM. Moreover, the RMSE in Table 2 also reveals that there is evident improvement in the proposed approach compare to RFM approach.

TABLE 2. Error of the checking points(NOTE: TPA, the proposed approach; EP_i , error of the i -th point; the unit in the table is cm , $1cm \approx 30$ pixels)

Approach	EP0	EP1	EP2	EP3	EP4	EP5	EP6	EP7	EP8	EP9	RMSE
TPA	0.105	0.074	0.170	0.100	0.242	0.242	0.000	0.314	0.199	0.120	0.396
RFM	0.105	0.074	0.328	0.167	0.242	0.242	0.000	0.314	0.170	0.100	0.417

5. Conclusions. We proposed a feature matching-based approach to measure the deformation field from MR images. The proposed approach uses matched feature point pairs to measure the local deformation, then interpolates the deformation field of every pixel via the deformation field of nodes of Dealunay triangles constructed using the corresponding points. The preliminary experiment results reveal that the proposed approach is effective. Advantages of the proposed approach include:

1). Comparison with the existed non-rigid registration approach, the proposed approach can be use in both image registration and deformation measurement areas.

2). Comparison with deformable models which used in the deformation measurement, the proposed featuring matching-based approach can measure deformation not only on the contour of object, but also in the inner of object.

3). The feature matching based approach for deformation measurement does not need the initial contour of an object. This is independent of the shape of the initial contour.

4). The proposed approach is more suitable for dense deformation fields measurement of non-rigid non-uniform object, due to take into account the local deformation direction information.

However, limitations need to be further addressed include:

1). The accuracy of deformation fields depends on the number of feature pairs in PMS, sparse feature pairs usually lower the accuracy of deformation fields. Therefore, the proposed approach will not be suitable for those data which cannot extract enough feature points.

2). False matches appeared in the PMS will affect the accuracy and reliability of obtained deformation fields. Therefore, good method needs to be proposed to remove false matches.

Acknowledgment. This work is partially supported by Prof. Shigerhiro Morikawa in Shiga University of Medical Science, Japan. The authors also gratefully acknowledge the helpful comments and suggestions of the reviewers, which have improved the presentation.

REFERENCES

- [1] Riederer, S. J., Current technical development of magnetic resonance imaging, *SIAM J. IEEE Engineering in Medicine and Biology*, vol.19, pp.34-41, 2000.
- [2] Matuszewski, B. J., J. K. Shen and L. K. Shark, Estimation of Internal Body Deformations Using an Elastic Registration Technique, *International Conference on Medical Information Visualisation-BioMedical Visualisation*, pp.15-20, 2006.
- [3] Cho, J. and P. J. Benkeser, Elastically deformable model-based motion-tracking of left ventricle, *The 26th Annual International Conference of the IEEE EMBS*, vol.1, pp.1925-1928, 2004.
- [4] Papademetris, X., A. J. Sinusas, D. P. Dione, R. T. Constable and J. S. Duncan, Estimation of 3-D left ventricular deformation from medical images using biomechanical models, *IEEE Transactions on Medical Imaging*, vol.21, pp.786-800, 2002.
- [5] Chenoune, Y., E. Delechelle, E. Petit, T. Goissen, J. Garot and A. Rahmouni, Segmentation of cardiac cine-MR images and myocardial deformation assessment using level set methods, *Computerized Medical Imaging and Graphics*, vol.29, pp.607-616, 2005.
- [6] Lang, J., D. K. Pai and R. J. Woodham, Robotic acquisition of deformable models, *IEEE International Conference on Robotics and Automation*, vol.1, pp.933-938, 2002.
- [7] Caselles, V., F. Catte, T. Coll and F. Dibos, A geometric model for active contours in image processing, *Numerische Mathematik*, vol.66, no.1, pp.1-31, 1993.
- [8] Malladi, R., J. A. Sethian and B. C. Vemuri, Shape modeling with front propagation: a level set approach, *IEEE Transactions on Pattern Analysis and Machine Intelligence*, vol.17, no.2, pp.158-175, 1995.
- [9] Caselles, V., Geometric models for active contours, *International Conference on Image Processing*, vol.3, pp.9-12, 1995.
- [10] Huang, F. Z. and J. B. Su, Face Contour Detection Using Geometric Active Contours, *Proceedings of the 4th World Congress on Intelligent Control and Automation*, vol.3, pp.2090-2093, 2002.
- [11] Kass, M. and A. Witkin, Snakes: active contours models, *IJOCV*, vol.1, no.4, pp.321-331, 1987.
- [12] Xu, C. Y., D. L. Pham and J. L. Prince, Image segmentation using deformable models, *Handbook of Medical Imaging*, pp.129-174, 2000.
- [13] Harris, C. and M. Stephens, A combined corner and edge detector, *Proceedings of The Fourth Alvey Vision Conference*, vol.1, no.4 pp.147-151, 1988.

- [14] Horn, B. K. P., Closed Form Solution of Absolute Orientation using Unit Quaternions, *Optical Society of America A: Optics, Image Science and Vision*, vol.4, pp.629-642, 1987.
- [15] Zhang, P. L., S.Hirai,K.Endo and S. Morikawa, Local Deformation Measurement of Biological Tissues Based on Feature Tracking of 3D MR Volumetric Images, *IEEE/ICME International Conference on Complex Medical Engineering*, pp.711-716, 2007.
- [16] Zhang, Y. F. and D. Doermann, Scene Labeling by Relaxation Operations, *IEEE TRANSACTIONS ON PATTERN ANALYSIS AND MACHINE INTELLIGENCE*, vol.28, pp.643-649, 2006.
- [17] Chen, G. Q., Robust Point Feature Matching In Projective Space, *Proceedings of the 2001 IEEE Computer Society Conference on Computer Vision and Pattern Recognition*, vol.1, pp.717-722, 2001.
- [18] Zhang, Z.Y., R. Deriche, O. Faugeras, and Q.-T. Luong. A robust technique for matching two uncalibrated images through the recovery of the unknown epipolar geometry. *Artificial Intelligence Journal. Also Research Report No.2273, INRIA Sophia-Antipolis.*, pp.87-119, 1995.
- [19] Xu, R. and Y. W.Chen, WAVELET-BASED MULTIREOLUTION MEDICAL IMAGE REGISTRATION STRATEGY COMBINING MUTUAL INFORMATION WITH SPATIAL INFORMATION, *International Journal of Innovative Computing, Information and Control*, vol.3, no.2, pp.285-296, 2007.